# Convergence of adaptive edge finite element methods for $\boldsymbol{H}(\mathbf{curl})-$elliptic problems

Liuqiang Zhong[a], Shi Shu[b], Long Chen[c], Jinchao Xu[d]

[a] School of Mathematics Sciences, South China Normal University, Guangzhou 510631, China

[b] School of Mathematical and Computational Sciences, Xiangtan University, Hunan 411105, China

[c] Department of Mathematics, University of California, Irvine, CA 92697, USA

[d] Department of Mathematics, Pennsylvania State University, University Park, PA 16802, USA

**Abstract**

The standard Adaptive Edge Finite Element Method (AEFEM), using first/second family Nédélec edge elements with any order, for the three dimensional $\boldsymbol{H}(\mathbf{curl})-$elliptic problems with variable coefficients is shown to be convergent for the sum of the energy error and the scaled error estimator. The special treatment of the data oscillation and the interior node property are removed from the proof. Numerical experiments indicate that the adaptive meshes and the associated numerical complexity are quasi-optimal.

Keywords: adaptive edge finite element method, convergence, $\boldsymbol{H}(\mathbf{curl})-$elliptic problems

## 1 Introduction

In this paper, we consider an adaptive edge finite element methods (AEFEMs) for solving the $\boldsymbol{H}(\mathbf{curl})-$elliptic problems: Find $\boldsymbol{u} \in H_0(\mathbf{curl};\Omega)$, such that

$$a(\boldsymbol{u},\boldsymbol{v}) = (\boldsymbol{g},\boldsymbol{v}) \quad \text{for all } \boldsymbol{v} \in H_0(\mathbf{curl};\Omega), \tag{1.1}$$

where

$$a(\boldsymbol{u},\boldsymbol{v}) = (\alpha\nabla\times\boldsymbol{u},\nabla\times\boldsymbol{v}) + (\beta\boldsymbol{u},\boldsymbol{v}), \tag{1.2}$$

and $(\cdot,\cdot)$ denotes the inner product in $\boldsymbol{L}^2(\Omega)$. The domain $\Omega\subset\mathbb{R}^3$ is a simply connected polyhedron and partitioned into non-overlapping subdomains $\Omega_i, 1\le i\le m$. We assume the modified material parameters $\alpha,\beta\in L^\infty(\Omega)\cap\prod_{i=1}^m W^{1,\infty}(\Omega_i)$, and $\alpha\ge\alpha_0>0,\beta\ge\beta_0>0$ for some constants $\alpha_0,\beta_0$, and $\boldsymbol{g}\in\prod_{i=1}^m H(\mathrm{div};\Omega_i)$.

Variational problems of the form (1.1) arises in many simulations of electromagnetic fields. For instance, it describes the eddy current model [6], and it is a core task in the time-domain simulation of electromagnetic fields if implicit time stepping is employed [14]. When variational problems of the form (1.1) describes the eddy current model, the parameter $\beta$ is related to the conductivity, and $\beta=0$ in the insulating regions. The assumption of $\beta$ in this paper excludes the above case.

The edge finite element methods using Nédélec edge finite elements [19, 20] for solving (1.1) is: Find $\boldsymbol{u}_\mathcal{T}\in\mathbb{V}(\mathcal{T})$, such that

$$a(\boldsymbol{u}_\mathcal{T},\boldsymbol{v}_\mathcal{T}) = (\boldsymbol{g},\boldsymbol{v}_\mathcal{T}), \quad \text{for all } \boldsymbol{v}_\mathcal{T}\in\mathbb{V}(\mathcal{T}), \tag{1.3}$$

where $\mathbb{V}(\mathcal{T})$ is the first or second types Nédélec element space (see §2 for details).

A broad class of problems in the form of (1.1) can cause strong singularities in the solution, for example, physical domains with non-trivial geometries, discontinuous material coefficients, and non-smooth source terms result in considerable computational problems. The singularity can be resolved by refine the mesh uniformly. The uniform refinement, however, will dramatically increase the computational effort including the physical memory as well as CPU time since the number of unknowns grows exponentially. On the other hand, local mesh refinement can also resolve the singularity by putting denser grids in where the function changes dramatically. The adaptive finite element method (AFEM) is such a methodology to distribute the grid points to optimize the relation between accuracy and computational labor (degrees of freedom).

In most of the existing work of adaptivity for computational electromagnetic fields [13, 26, 17, 25, 1], researchers focus on the engineering simulations. We are interested in the theoretical understanding of the adaptive edge finite element methods for solving (1.3). We shall prove the convergence of the following procedure of adaptive edge finite element methods (AEFEM)

$$\textbf{SOLVE} \rightarrow \textbf{ESTIMATE} \rightarrow \textbf{MARK} \rightarrow \textbf{REFINE}. \tag{1.4}$$

There are only few research results for the convergence of the adaptive procedure for Maxwell's type equations. In [7] and [16], the authors prove the convergence for the two- and three-dimensional eddy currents equations, respectively. In these work, the so-called interior node property and marking for oscillation are imposed as technical assumptions while they are not required in the practical computation. In addition only the first family of Nédélec linear edge elements is considered in these work. Compared with existing work [7, 16], our contributions in this paper are to

- prove the convergence without the restrictive interior node property and the extra marking of data oscillation;
- generalize to high order and two types of Nédélec edge elements.

We summarize our main result in the following theorem.

**Theorem 1.1 (Convergence)** *Let $\{\mathcal{T}_k, \mathbb{V}(\mathcal{T}_k), \boldsymbol{u}_k, \eta_k\}$ be the sequence of meshes, finite element spaces, discrete solutions and error estimators produced by AEFEM. Then there exist constants $\rho > 0$ and $\delta \in (0,1)$, depending only on marking parameter, the shape regularity of the initial mesh, the coefficients $\alpha$ and $\beta$, such that*

$$\|\boldsymbol{u} - \boldsymbol{u}_{k+1}\|_A^2 + \rho\eta_{k+1}^2 \le \delta\left(\|\boldsymbol{u} - u_k\|_A^2 + \rho\eta_k^2\right).$$

As a consequence, AEFEM will converge in finite steps for a given tolerance.

To avoid the repeated use of generic but unspecified constants, following [27], we shall use the following short-hand notation: $x \lesssim y$ means $x \le Cy$, where constant $C$ is a generic positive constant independent of the variables that appear in the inequalities and especially the mesh parameters. The notation $C_i$, with subscript, denotes specific important constants.

The remainder of the article is organized as follows. In the next section, we introduce some preliminaries about Sobolev spaces, finite element spaces, and the bilinear form $a(\cdot,\cdot)$. We present the adaptive algorithm and describe each procedure of (1.4) in §3. We prove the convergence of AEFEM in §4 and report some numerical results in support of theoretical ones in §5.

## 2 Prelimimaries

Let $\Omega \subseteq \mathbb{R}^3$ be a simply connected polyhedron with boundary $\partial\Omega$ and unit outward normal $\boldsymbol{n}_{\partial\Omega}$. For any set $G \subset \mathbb{R}^3$ with nonempty interior, $L^2(G)$ (resp. $\boldsymbol{L}^2(G)$) stands for the Hilbert space of square integrable functions (resp. vector fields) on $G$ with inner product $(\cdot,\cdot)_G$, and $H^1(G) := \{v \in L^2(G) : \nabla v \in \boldsymbol{L}^2(G)\}$. We also define the spaces

$$\begin{aligned} \boldsymbol{H}(\mathbf{curl}; G) &= \left\{\boldsymbol{v} \in \boldsymbol{L}^2(G) \;\middle|\; \nabla \times \boldsymbol{v} \in \boldsymbol{L}^2(G)\right\}, \\ \boldsymbol{H}(\mathrm{div}; G) &= \left\{\boldsymbol{v} \in \boldsymbol{L}^2(G) \;\middle|\; \nabla \cdot \boldsymbol{v} \in L^2(G)\ \right\}, \end{aligned}$$

equipped with norms

$$\begin{aligned} \|\boldsymbol{v}\|_{\mathbf{curl};G} &= \left(\|\boldsymbol{v}\|_{0;G}^2 + \|\nabla \times \boldsymbol{v}\|_{0;G}^2\right)^{1/2}, \quad \text{for } \boldsymbol{v} \in \boldsymbol{H}(\mathbf{curl}; G), \\ \|\boldsymbol{v}\|_{\mathrm{div};G} &= \left(\|\boldsymbol{v}\|_{0;G}^2 + \|\nabla \cdot \boldsymbol{v}\|_{0;G}^2\right)^{1/2}, \quad \text{for } \boldsymbol{v} \in \boldsymbol{H}(\mathrm{div}; G), \end{aligned}$$

respectively, where $\|\cdot\|_{0;G} := (\cdot,\cdot)_G^{1/2}$ denotes the norm of the space $\boldsymbol{L}^2(G)$ or $L^2(G)$. Especially, we define $H_0^1(G) := \{u \in H^1(G), u|_{\partial G} = 0\}$ and $\boldsymbol{H}_0(\mathbf{curl}; G) = \{\boldsymbol{u} \in \boldsymbol{H}(\mathbf{curl}; G), \boldsymbol{n}_{\partial G} \times \boldsymbol{u} = \mathbf{0}$ on $\partial G\}$ in the trace sense, where $\boldsymbol{n}_{\partial G}$ denotes the unit outward normal of the boundary $\partial G$ of domain $G$. We omit the subscript if $G = \Omega$ for simplicity.

We consider a shape regular tetrahedral triangulation $\mathcal{T}$ of $\Omega$ which is consistent with the partition $\bar{\Omega} = \prod_{i=1}^m \bar{\Omega}_i$ in the sense that each $\Omega_i, 1 \le i \le m$, inherits a shape regular tetrahedral triangulation $\mathcal{T}(\Omega_i)$. For each integer $l > 0$, the $l^{th}$ order element of the first family and the second family of Nédélec elements generate the following two spaces:

$$\begin{aligned} \mathbb{V}^{l,1}(\mathcal{T}) &:= \Big\{\boldsymbol{v}_h^{l,1} \in H_0(\mathbf{curl}; \Omega) \;\Big|\; \boldsymbol{v}_h^{l,1}|_\tau \in (\mathcal{P}_{l-1})^3 \oplus \{\boldsymbol{p} \in (\tilde{P}_l)^3 \mid \boldsymbol{p}(\boldsymbol{x}) \cdot \boldsymbol{x} = 0\} \\ &\qquad \text{for all } \tau \in \mathcal{T}\Big\}, \\ \mathbb{V}^{l,2}(\mathcal{T}) &:= \Big\{\boldsymbol{v}_h^{l,2} \in H_0(\mathbf{curl}; \Omega) \;\Big|\; \boldsymbol{v}_h^{l,2}|_\tau \in (\mathcal{P}_l)^3 \text{ for all } \tau \in \mathcal{T}\Big\}, \end{aligned}$$

where $\mathcal{P}_l$ denotes the standard space of polynomials of total degree less than or equal to $l$, and $\tilde{\mathcal{P}}_l$ the space of homogeneous polynomials of degree $l$.

The bilinear form $a(\cdot,\cdot)$ restricted to the domain $G \subseteq \Omega$ is denoted by $a_G(\cdot,\cdot)$. It is easy to show that the bilinear fulfills the local continuity

$$a_G(\boldsymbol{v}, \boldsymbol{w}) \le C_{a;G}\|\boldsymbol{v}\|_{\mathbf{curl};G}\|\boldsymbol{w}\|_{\mathbf{curl};G}, \qquad \text{for any } \boldsymbol{v}, \boldsymbol{w} \in \boldsymbol{H}(\mathbf{curl}; G), \tag{2.5}$$

where constant $C_{a;G} := \max\{\|\alpha\|_{\infty,G}, \|\beta\|_{\infty,G}\}$. When $G = \Omega$, we simply denoted by $C_a := C_{a;G}$. Furthermore, let $c_a := \min\{\alpha_0, \beta_0\}$, we have

$$a(\boldsymbol{v}, \boldsymbol{v}) \ge c_a\|\boldsymbol{v}\|_{\mathbf{curl};\Omega}^2, \quad \text{for all } \boldsymbol{v} \in \boldsymbol{H}_0(\mathbf{curl}; G). \tag{2.6}$$

Combing (2.6) with the symmetry of $a_G(\cdot,\cdot)$, the bilinear form induces the following energy norm

$$\|\boldsymbol{v}\|_{A;G}^2 = a_G(\boldsymbol{v}, \boldsymbol{v}), \qquad \text{for } \boldsymbol{v} \in H_0(\mathbf{curl}; \Omega). \tag{2.7}$$

When $G = \Omega$, we omit the subscript $\Omega$, i.e., $\|\boldsymbol{v}\|_A = \|\boldsymbol{v}\|_{A;\Omega}$.

To save notation, we use $\mathbb{V}(\mathcal{T})$ for the first or second types Nédélec element space which will be clear in the context. The lowest order element of the first family $\mathbb{V}^{1,1}(\mathcal{T})$ is the simplest and thus most popular edge element space, and $\mathbb{V}^{1,1}(\mathcal{T}) \subseteq \mathbb{V}(\mathcal{T})$ is always true.

# 3 Adaptive Edge Finite Element Method

In this section, we shall present an adaptive edge finite element method for solving the $\boldsymbol{H}(\mathbf{curl})-$elliptic problems (1.1). We use local mesh refinement to resolve the possible singularity in the solution.

Our adaptive edge finite element method is presented in the following subroutine:

```
[u_J, T_J] = AEFEM (T_0, g, tol, θ)

 AEFEM compute an approximation u_J by adaptive edge finite element methods.
 Input: T_0 initial triangulation; g data; tol stopping criteria; θ between (0,1).
 Output: u_J finite element approximation; T_J the finest mesh.

 η = 1, k = 0;
 while η ≥ tol
     k = k + 1;
     SOLVE equation (1.3) on T_k to get the solution u_k;
     ESTIMATE the error by η = η(u_k, T_k);
     MARK a set M_k ⊂ T_k with minimum number such that η^2(u_k, M_k) ≥ θ η^2(u_k, T_k);
     REFINE element τ ∈ M_k and necessary elements to get a conforming grid T_{k+1};
 end
 u_J = u_k; T_J = T_k;
```

The goal of this paper is to prove that the algorithm AEFEM will terminate in finite steps for a given tolerance. Our algorithm is adapted from the algorithm for second order elliptic PDEs in [8]. It is the simplest adaptive algorithm in the sense that no marking for oscillation and no interior node property should be enforced in the mark and refine procedure.

In the following subsections, we shall discuss each step in AEFEM in detail.

## 3.1 Procedure SOLVE

For a given function $\boldsymbol{g} \in \prod_{i=1}^{m} H(\mathrm{div}; \Omega_i)$ and a given mesh $\mathcal{T}$, we suppose that the module **SOLVE** outputs the exact discrete solution $\boldsymbol{u}_{\mathcal{T}} \in \mathbb{V}(\mathcal{T})$ of (1.3):

$$\boldsymbol{u}_{\mathcal{T}} = \mathbf{SOLVE}(\mathcal{T}, \boldsymbol{g}).$$

Here, we assume that the solutions of the finite dimensional problems can be solved to any accurately and efficiently. Examples of such optimal solvers include multigrid methods [14, 2, 3, 23]. Note that the above studies focus on quasi-uniform grids. Multigrid methods for the $\boldsymbol{H}(\mathbf{curl})$ problems on adaptive grids can be found in recent work [15, 10].

## 3.2 Procedure ESTIMATE

For the $\boldsymbol{H}(\mathbf{curl})$-system, efficient and reliable a posteriori error estimators have been widely developed and analyzed in [3, 4, 5, 22]. A posteriori error estimators based on the separate treatment of the kernel of the **curl**-operator and its orthogonal complement were presented in [3]. A residual type and a hierarchical type a posteriori error estimator were proposed and analyzed under certain conditions on the domain in [4, 5]. Recently, the reliability of the residual type error estimator on Lipschitz domains was established in [22] using the commuting quasi-interpolation operators introduced in [21].

We shall use a residual type a posterior error estimator which is similar to that in [22]. Given a conforming triangulation $\mathcal{T}$, let $\mathcal{F}(\mathcal{T})$ denote the set of the interior faces of $\mathcal{T}$ with a fixed orientation. For any face $f \in \mathcal{F}(\mathcal{T})$ shared by two elements $\tau_1$ and $\tau_2$, i.e., $\partial\tau_1 \cap \partial\tau_2 = f$ with the orientation of $f$ being consistent with that of $\tau_1$, we define the interelement jumps of a scalar function $w$ across $f$ as

$$[\![w]\!] \quad = \quad w|_{\tau_1} - w|_{\tau_2}.$$

For $\tau \in \mathcal{T}, f \in \mathcal{F}(\mathcal{T})$ and $\boldsymbol{v}_\mathcal{T} \in \mathbb{V}(\mathcal{T})$, we define the following element-wise residuals and face-wise jump residuals associated with interior faces as

$$\begin{aligned}
R_1(\boldsymbol{v}_\mathcal{T})|_\tau &:= \boldsymbol{g}|_\tau - (\nabla \times (\alpha \nabla \times \boldsymbol{v}_\mathcal{T}) + \beta \boldsymbol{v}_\mathcal{T})|_\tau, && (3.1)\\
R_2(\boldsymbol{v}_\mathcal{T})|_\tau &:= \nabla \cdot (\boldsymbol{g}|_\tau - \beta \boldsymbol{v}_\mathcal{T}|_\tau), && (3.2)\\
J_1(\boldsymbol{v}_\mathcal{T})|_f &:= [\![(\alpha \nabla \times \boldsymbol{v}_\mathcal{T}) \times \boldsymbol{n}_f]\!], && (3.3)\\
J_2(\boldsymbol{v}_\mathcal{T})|_f &:= [\![(\boldsymbol{g} - \beta \boldsymbol{v}_\mathcal{T}) \cdot \boldsymbol{n}_f]\!]. && (3.4)
\end{aligned}$$

**Remark 3.1** *Although we include $\alpha, \beta$, and $\boldsymbol{g}$ in the definitions of $R_j$ and $J_i (j = 1, 2)$, we skip the explicit dependence in the notation since they are fixed for all triangulations.*

The error estimate for $\boldsymbol{v}_\mathcal{T} \in \mathbb{V}(\mathcal{T})$ on $\tau \in \mathcal{T}$ is given by

$$\begin{aligned}
\eta^2_\mathcal{T}(\boldsymbol{v}_\mathcal{T}, \tau) \quad := \quad & h^2_\tau \left( \|R_1(\boldsymbol{v}_\mathcal{T})\|^2_{0;\tau} + \|R_2(\boldsymbol{v}_\mathcal{T})\|^2_{0;\tau} \right) \\
& + \sum_{f \in \tau \cap \mathcal{F}(\mathcal{T})} h_\tau \left( \|J_1(\boldsymbol{v}_\mathcal{T})\|^2_{0,f} + \|J_2(\boldsymbol{v}_\mathcal{T})\|^2_{0,f} \right), \qquad (3.5)
\end{aligned}$$

where $h_\tau := |\tau|^{1/3}$ measures the local mesh size of the element $\tau$.

In these element-wise or face-wise terms, a correct scaling is used to shift the norm from $L^2$-norm to a correct dual norm. Note that even for jump terms across the face, the size $h_\tau$ is used. Although $h_\tau$ and $h_f$, the diameter of $f$, are comparable, the use of $h_\tau$ is crucial for the reduction of the error estimator, as we can see from the proof of Lemma 4.5.

For any subset $\mathcal{M} \subseteq \mathcal{T}$, we define

$$\eta^2_\mathcal{T}(\boldsymbol{v}_\mathcal{T}, \mathcal{M}) = \sum_{\tau \in \mathcal{M}} \eta^2_\mathcal{T}(\boldsymbol{v}_\mathcal{T}, \tau). \qquad (3.6)$$

When $\mathcal{M} = \mathcal{T}$, we shall simplify the notation as $\eta(\boldsymbol{v}_\mathcal{T}, \mathcal{T})$.

We assume that, given a triangulation $\mathcal{T}$ and the corresponding discrete solution $\boldsymbol{u}_\mathcal{T} \in \mathbb{V}(\mathcal{T})$ of (1.3), the module **ESTIMATE** outputs the estimates $\eta_\mathcal{T}(\boldsymbol{v}_\mathcal{T}, \tau)$ for all $\tau \in \mathcal{T}$.

## 3.3 Procedure MARK

In the selection of elements we rely on the Dörfler marking [12]. Given a triangulation $\mathcal{T}$, a set of estimates $\{\eta_\mathcal{T}(\boldsymbol{u}_\mathcal{T}, \tau)\}_{\tau \in \mathcal{T}}$, and a marking parameter $\theta \in (0, 1)$, we suppose that the module **MARK** outputs a subset of marked elements $\mathcal{M} \subset \mathcal{T}$ with minimal cardinality, such that

$$\eta^2_\mathcal{T}(\boldsymbol{u}_\mathcal{T}, \mathcal{M}) \geq \theta \eta^2(\boldsymbol{u}_\mathcal{T}, \mathcal{T}). \qquad (3.7)$$

## 3.4 Procedure REFINE

Starting from an initial triangulation $\mathcal{T}_0$, $\mathcal{T}_{k+1}$ is obtained from $\mathcal{T}_k$ by a local mesh refinement method. We denote by

$$\mathscr{C}(\mathcal{T}_0) = \{\mathcal{T} : \mathcal{T} \text{ is conforming and refined from } \mathcal{T}_0\},$$

and $\mathcal{T}_1 \leq \mathcal{T}_2$ if $\mathcal{T}_2$ is a refinement of $\mathcal{T}_1$.

We assume that each element $\tau \in \mathcal{M}_k$, the marked element set in $\mathcal{T}_k$, is at least divided into two equal volume parts and $\mathcal{T}_{k+1}$ and $\mathcal{T}_k$ are nested in the sense that $\mathbb{V}(\mathcal{T}_k) \subset \mathbb{V}(\mathcal{T}_{k+1})$. We also assume that the class $\mathscr{C}(\mathcal{T}_0)$ is uniformly shape regular in the sense of [11].

# 4 Convergence of AEFEM

In this section, we will prove that the algorithm `AEFEM` will converge by showing that the sum of the energy error and the scaled error estimator, between two consecutive adaptive loops, is a contraction.

## 4.1 Orthogonality

**Theorem 4.1** *For $\mathcal{T}, \mathcal{T}_* \in \mathscr{C}(\mathcal{T}_0)$ with $\mathcal{T} \leq \mathcal{T}_*$, let $\boldsymbol{u}_{\mathcal{T}} \in \mathbb{V}(\mathcal{T})$ and $\boldsymbol{u}_{\mathcal{T}_*} \in \mathbb{V}(\mathcal{T}_*)$ be the discrete solutions of (1.3). Then we have*

$$\|\boldsymbol{u} - \boldsymbol{u}_{\mathcal{T}_*}\|_A^2 = \|\boldsymbol{u} - \boldsymbol{u}_{\mathcal{T}}\|_A^2 - \|\boldsymbol{u}_{\mathcal{T}_*} - \boldsymbol{u}_{\mathcal{T}}\|_A^2. \tag{4.1}$$

**Proof.** The proof of this theorem is straightforward by using the definition of the energy norm and the following Galerkin orthogonality

$$a(\boldsymbol{u} - \boldsymbol{u}_{\mathcal{T}_*}, \boldsymbol{u}_{\mathcal{T}_*} - \boldsymbol{u}_{\mathcal{T}}) = 0. \tag{4.2}$$

∎

## 4.2 Residual type error estimate: upper bound

Before we prove the reliability of the residual type error estimator, we introduce a Clément-type quasi-interpolation operator [21] and the corresponding approximation error estimate.

**Theorem 4.2 (Thm 1 of [22])** *There exists an operator $\Pi_{\mathcal{T}}^S : H_0(\mathbf{curl};\Omega) \to \mathbb{V}^{1,1}(\mathcal{T})$ with the following properties: For every $\boldsymbol{v} \in H_0(\mathbf{curl};\Omega)$, there exist $\varphi \in H_0^1(\Omega)$ and $\boldsymbol{z} \in (H_0^1(\Omega))^3$, such that*

$$\boldsymbol{v} - \Pi_{\mathcal{T}}^S \boldsymbol{v} = \nabla\varphi + \boldsymbol{z}, \tag{4.3}$$

*The decompositon satisfies*

$$\begin{aligned} h_\tau \|\varphi\|_{0,\tau} + \|\nabla\varphi\|_{0,\tau} &\lesssim \|\boldsymbol{v}\|_{0;\tilde{\Omega}_\tau}, & (4.4)\\ h_\tau \|\boldsymbol{z}\|_{0,\tau} + \|\nabla\boldsymbol{z}\|_{0,\tau} &\lesssim \|\nabla\times\boldsymbol{v}\|_{0;\tilde{\Omega}_\tau}, & (4.5)\end{aligned}$$

*where the constants depend only on the shape of the elements in the enlarged element patch $\tilde{\Omega}_\tau$ of element $\tau$ ( more detail of the corresponding definition can be found in [22]), but does not depend on the global shape of the domain $\Omega$ or the size of $\tilde{\Omega}_\tau$.*

Combining the standard tools for the residual-type a posteriori error analysis with the Clément-type commuting quasi-interpolation in [16], it is easy to obtain the following upper bound. More details can be found in Corollary 2 of [22].

**Lemma 4.3 (Global a posteriori upper bound)** *Let $\boldsymbol{u} \in H_0(\mathbf{curl};\Omega)$ be the solution of (1.1), $\mathcal{T} \in \mathscr{C}(\mathcal{T}_0)$, and $\boldsymbol{u}_\mathcal{T} \in \mathbb{V}(\mathcal{T})$ be the discrete solution of (1.3). Then there exists a constant $C_1 > 0$ depending only on $c_a^{-1} = \max\{\alpha_0^{-1}, \beta_0^{-1}\}$ and the shape regularity of $\mathcal{T}$, such that*

$$\|\boldsymbol{u} - \boldsymbol{u}_\mathcal{T}\|_A^2 \leq C_1 \eta^2(\boldsymbol{u}_\mathcal{T}, \mathcal{T}). \tag{4.6}$$

**Proof.** The coercivity of $a(\cdot,\cdot)$ and the Galerkin orthogonality imply that

$$\|\boldsymbol{u} - \boldsymbol{u}_\mathcal{T}\|_A \leq \sup_{\boldsymbol{v} \in H_0(\mathbf{curl};\Omega)} \frac{a(\boldsymbol{u} - \boldsymbol{u}_\mathcal{T}, \boldsymbol{v})}{\|\boldsymbol{v}\|_A} \tag{4.7}$$

We apply Theorem 4.2 to decompose $\boldsymbol{v} - \Pi_\mathcal{T}^S \boldsymbol{v} = \nabla\varphi + \boldsymbol{z}$ satisfying the corresponding norm estimates (4.4) and (4.5), then using the Green formula, the trace inequality $h_f^{-1}\|\phi\|_{0,f}^2 \lesssim h_f^{-2}\|\phi\|_{0,\tau}^2 + \|\nabla\phi\|_{0,\tau}^2$, and shape regularity of the mesh $h_f \lesssim h_\tau$. Therefore, we have

$$\begin{aligned}
a(\boldsymbol{u} - \boldsymbol{u}_\mathcal{T}, \boldsymbol{v}) &= a(\boldsymbol{u} - \boldsymbol{u}_\mathcal{T}, \boldsymbol{v} - \Pi_\mathcal{T}^S \boldsymbol{v}) = a(\boldsymbol{u} - \boldsymbol{u}_\mathcal{T}, \boldsymbol{z} + \nabla\varphi) \\
&= (\boldsymbol{g}, \boldsymbol{z} + \nabla\varphi) - a(\boldsymbol{u}_\mathcal{T}, \boldsymbol{z} + \nabla\varphi) \\
&= \sum_{\tau \in \mathcal{T}} \Big( (\boldsymbol{g}, \boldsymbol{z} + \nabla\varphi)_{0,\tau} - (\alpha\nabla \times \boldsymbol{u}_\mathcal{T}, \nabla \times \boldsymbol{z})_{0,\tau} - (\beta \boldsymbol{u}_\mathcal{T}, \boldsymbol{z} + \nabla\varphi)_{0,\tau} \Big) \\
&= \sum_{\tau \in \mathcal{T}} \Big( (R_1(\boldsymbol{u}_\mathcal{T}), \boldsymbol{z})_{0,\tau} - (R_2(\boldsymbol{u}_\mathcal{T}), \varphi)_{0,\tau} \Big) \\
&\quad + \sum_{f \in \mathcal{F}(\mathcal{T})} \Big( (J_1(\boldsymbol{u}_\mathcal{T}), \boldsymbol{z})_{0,f} + (J_2(\boldsymbol{u}_\mathcal{T}), \varphi)_{0,f} \Big) \\
&= \sum_{\tau \in \mathcal{T}} \Big( \|R_1(\boldsymbol{u}_\mathcal{T})\|_{0,\tau} \|\boldsymbol{z}\|_{0,\tau} + \|R_2(\boldsymbol{u}_\mathcal{T})\|_{0,\tau} \|\varphi\|_{0,\tau} \Big) \\
&\quad + \sum_{f \in \mathcal{F}(\mathcal{T})} \Big( \|J_1(\boldsymbol{u}_\mathcal{T})\|_{0,f} \|\boldsymbol{z}\|_{0,f} + \|J_2(\boldsymbol{u}_\mathcal{T})\|_{0,f} \|\varphi\|_{0,f} \Big) \\
&\lesssim \eta(\boldsymbol{u}_\mathcal{T}, \mathcal{T}) c_a^{-1} \|\boldsymbol{v}\|_A
\end{aligned} \tag{4.8}$$

The desired estimate (4.6) is a direct consequence of (4.7) and (4.8). ∎

## 4.3 Contraction of the error estimator

In this subsection, we shall prove the contraction of the error estimator. To this end, we need to define the weighted maximum-norm of the coefficients $\alpha$ and $\beta$ as follows

$$\eta_\mathcal{T}^2(\boldsymbol{D}, \tau) \quad := \quad h_\tau^2 \left( \|\nabla\alpha\|_{\infty;\tau}^2 + h_\tau^{-2}\|\alpha\|_{\infty;\Omega_\tau}^2 + \|\nabla\beta\|_{\infty;\tau}^2 + h_\tau^{-2}\|\beta\|_{\infty;\Omega_\tau}^2 \right),$$

where $\Omega_\tau = \{\tau' \in \mathcal{T}, \tau' \cap \tau \neq \varnothing\}$. For any subset $\mathcal{M} \subseteq \mathcal{T}$, we define

$$\eta_\mathcal{T}(\boldsymbol{D}, \mathcal{M}) \quad := \quad \max_{\tau \in \mathcal{M}} \eta_\mathcal{T}(\boldsymbol{D}, \tau).$$

When $\mathcal{M} = \mathcal{T}$, we shall simplify the notation as $\eta(\boldsymbol{D}, \mathcal{T}) := \eta_\mathcal{T}(\boldsymbol{D}, \mathcal{T})$.

In view of the above definitions, for $\mathcal{T} \leq \mathcal{T}_*$ and $\mathcal{T}, \mathcal{T}_* \in \mathscr{C}(\mathcal{T}_0)$, the following monotonicity property holds

$$\eta(\boldsymbol{D}, \mathcal{T}_*) \leq \eta(\boldsymbol{D}, \mathcal{T}) \leq \eta(\boldsymbol{D}, \mathcal{T}_0). \tag{4.9}$$

Let us first consider the effect of changing the finite element function used in the estimator.

**Lemma 4.4** *For $\mathcal{T}, \mathcal{T}_* \in \mathscr{C}(\mathcal{T}_0)$ with $\mathcal{T} \leq \mathcal{T}_*$, let $\boldsymbol{v}_\mathcal{T} \in \mathbb{V}(\mathcal{T})$ and $\boldsymbol{v}_{\mathcal{T}_*} \in \mathbb{V}(\mathcal{T}_*)$. Then for any $\epsilon > 0$, there exists a constant $C_\epsilon > 0$, such that*

$$\eta^2(\boldsymbol{v}_{\mathcal{T}_*}, \mathcal{T}_*) \leq (1+\epsilon)\eta^2(\boldsymbol{v}_\mathcal{T}, \mathcal{T}_*) + C_\epsilon \eta^2(\boldsymbol{D}, \mathcal{T}_0)\|\boldsymbol{v}_{\mathcal{T}_*} - \boldsymbol{v}_\mathcal{T}\|^2_{\mathbf{curl};\Omega}. \tag{4.10}$$

**Proof.** For each $\tau_* \in \mathcal{T}_*$, we will consider the four terms in $\eta^2_{\mathcal{T}_*}(\boldsymbol{v}_{\mathcal{T}_*}, \tau_*)$ one by one.

a) We first deal with the element residuals $R_1(\boldsymbol{v}_{\mathcal{T}_*})$ and $R_2(\boldsymbol{v}_{\mathcal{T}_*})$. Using the definition of $R_1(\boldsymbol{v}_{\mathcal{T}_*})$, the triangle inequality and the inverse inequality, we have

$$\begin{aligned}
h_{\tau_*}\|R_1(\boldsymbol{v}_{\mathcal{T}_*})\|_{0;\tau_*} &\leq h_{\tau_*}\left(\|\boldsymbol{g} - \mathcal{L}\boldsymbol{v}_\mathcal{T}\|_{0;\tau_*} + \|\mathcal{L}(\boldsymbol{v}_\mathcal{T} - \boldsymbol{v}_{\mathcal{T}_*})\|_{0;\tau_*}\right) \\
&\leq h_{\tau_*}\Big(\|R_1(\boldsymbol{v}_\mathcal{T})\|_{0;\tau_*} + \|\nabla \times (\alpha \nabla \times (\boldsymbol{v}_\mathcal{T} - \boldsymbol{v}_{\mathcal{T}_*}))\|_{0;\tau_*} \\
&\quad + \|\beta(\boldsymbol{v}_\mathcal{T} - \boldsymbol{v}_{\mathcal{T}_*})\|_{0;\tau_*}\Big),
\end{aligned} \tag{4.11}$$

where $\mathcal{L}\boldsymbol{v}_\mathcal{T} := \nabla \times (\alpha \nabla \times \boldsymbol{v}_\mathcal{T}) + \beta \boldsymbol{v}_\mathcal{T}$.

Making use of the following chain rule

$$\nabla \times (\alpha \nabla \times (\boldsymbol{v}_\mathcal{T} - \boldsymbol{v}_{\mathcal{T}_*})) = \alpha \nabla \times (\nabla \times (\boldsymbol{v}_\mathcal{T} - \boldsymbol{v}_{\mathcal{T}_*})) + (\nabla \alpha) \times (\nabla \times (\boldsymbol{v}_\mathcal{T} - \boldsymbol{v}_{\mathcal{T}_*})),$$

the triangle inequality, the inverse inequality, and the discrete Hölder inequality, we have

$$\begin{aligned}
&\|\nabla \times (\alpha \nabla \times (\boldsymbol{v}_\mathcal{T} - \boldsymbol{v}_{\mathcal{T}_*}))\|_{0;\tau_*} + \|\beta(\boldsymbol{v}_\mathcal{T} - \boldsymbol{v}_{\mathcal{T}_*})\|_{0;\tau_*} \\
&\quad \leq \|\alpha \nabla \times (\nabla \times (\boldsymbol{v}_\mathcal{T} - \boldsymbol{v}_{\mathcal{T}_*}))\|_{0;\tau_*} + \|(\nabla \alpha) \times (\nabla \times (\boldsymbol{v}_\mathcal{T} - \boldsymbol{v}_{\mathcal{T}_*}))\|_{0;\tau_*} + \|\beta(\boldsymbol{v}_\mathcal{T} - \boldsymbol{v}_{\mathcal{T}_*})\|_{0;\tau_*} \\
&\quad \lesssim \|\alpha\|_{\infty,\tau_*} h^{-1}_{\tau_*}\|\nabla \times (\boldsymbol{v}_\mathcal{T} - \boldsymbol{v}_{\mathcal{T}_*})\|_{0;\tau_*} + \|\nabla \alpha\|_{\infty;\tau_*}\|\nabla \times (\boldsymbol{v}_\mathcal{T} - \boldsymbol{v}_{\mathcal{T}_*})\|_{0;\tau_*} \\
&\qquad + \|\beta\|_{\infty,\tau_*}\|\boldsymbol{v}_\mathcal{T} - \boldsymbol{v}_{\mathcal{T}_*}\|_{0;\tau_*} \\
&\quad \lesssim h^{-1}_{\tau_*}\eta_{\mathcal{T}_*}(\boldsymbol{D}, \tau_*)\|\boldsymbol{v}_{\mathcal{T}_*} - \boldsymbol{v}_\mathcal{T}\|_{\mathbf{curl};\tau_*}.
\end{aligned} \tag{4.12}$$

Substituting (4.12) into (4.11), we obtain

$$h_{\tau_*}\|R_1(\boldsymbol{v}_{\mathcal{T}_*})\|_{0;\tau_*} \lesssim h_{\tau_*}\|R_1(\boldsymbol{v}_\mathcal{T})\|_{0;\tau_*} + \eta_{\mathcal{T}_*}(\boldsymbol{D}, \tau_*)\|\boldsymbol{v}_{\mathcal{T}_*} - \boldsymbol{v}_\mathcal{T}\|_{\mathbf{curl};\tau_*}. \tag{4.13}$$

For $R_2(\boldsymbol{v}_{\mathcal{T}_*})$, using another chain rule

$$\nabla \cdot [\beta(\boldsymbol{v}_\mathcal{T} - \boldsymbol{v}_{\mathcal{T}_*})] = \beta \nabla \cdot (\boldsymbol{v}_\mathcal{T} - \boldsymbol{v}_{\mathcal{T}_*}) + (\nabla \beta) \cdot (\boldsymbol{v}_\mathcal{T} - \boldsymbol{v}_{\mathcal{T}_*})$$

and a similar method for proving (4.12), we get

$$\begin{aligned}
h_{\tau_*}\|R_2(\boldsymbol{v}_{\mathcal{T}_*})\|_{0;\tau_*} &\leq h_{\tau_*}\left(\|\nabla \cdot (\boldsymbol{g} - \beta \boldsymbol{v}_\mathcal{T})\|_{0;\tau_*} + \|\nabla \cdot [\beta(\boldsymbol{v}_\mathcal{T} - \boldsymbol{v}_{\mathcal{T}_*})]\|_{0;\tau_*}\right) \\
&\leq h_{\tau_*}\Big(\|R_2(\boldsymbol{v}_\mathcal{T})\|_{0;\tau_*} \\
&\quad + \|\beta \nabla \cdot (\boldsymbol{v}_\mathcal{T} - \boldsymbol{v}_{\mathcal{T}_*})\|_{0;\tau_*} + \|(\nabla \beta) \cdot (\boldsymbol{v}_\mathcal{T} - \boldsymbol{v}_{\mathcal{T}_*})\|_{0;\tau_*}\Big) \\
&\lesssim h_{\tau_*}\Big(\|R_2(\boldsymbol{v}_\mathcal{T})\|_{0;\tau_*} + \|\beta\|_{\infty;\tau_*} h^{-1}_{\tau_*}\|\boldsymbol{v}_\mathcal{T} - \boldsymbol{v}_{\mathcal{T}_*}\|_{0;\tau_*} \\
&\quad + \|\nabla \beta\|_{\infty,\tau_*}\|\boldsymbol{v}_\mathcal{T} - \boldsymbol{v}_{\mathcal{T}_*}\|_{0;\tau_*}\Big) \\
&\leq h_{\tau_*}\|R_2(\boldsymbol{v}_\mathcal{T})\|_{0;\tau_*} + \eta_{\mathcal{T}_*}(\boldsymbol{D}, \tau_*)\|\boldsymbol{v}_{\mathcal{T}_*} - \boldsymbol{v}_\mathcal{T}\|_{0;\tau_*}.
\end{aligned} \tag{4.14}$$

b) Now, we consider the jump residuals $J_1(\boldsymbol{v}_{\mathcal{T}_*})$ and $J_2(\boldsymbol{v}_{\mathcal{T}_*})$ associated with interior faces. For each $f_* \in \mathcal{F}(\mathcal{T}_*)$, where $f_* = \tau_*^1 \cap \tau_*^2$ with $\tau_*^1, \tau_*^2 \in \mathcal{T}_*$, using the definition of $J_1(\boldsymbol{v}_{\mathcal{T}_*})$ and the triangle inequality, we have

$$h_{\tau_*}^{1/2}\|J_1(\boldsymbol{v}_{\mathcal{T}_*})\|_{0;f_*} \le h_{\tau_*}^{1/2}\|J_1(\boldsymbol{v}_{\mathcal{T}})\|_{0;f_*} + h_{\tau_*}^{1/2}\|[\![(\alpha\nabla\times(\boldsymbol{v}_{\mathcal{T}_*}-\boldsymbol{v}_{\mathcal{T}}))\times\boldsymbol{n}]\!]\|_{0;f_*}. \tag{4.15}$$

The standard scaling argument implies

$$\begin{aligned}
&h_{\tau_*}^{1/2}\|[\![(\alpha\nabla\times(\boldsymbol{v}_{\mathcal{T}_*}-\boldsymbol{v}_{\mathcal{T}}))\times\boldsymbol{n}]\!]\|_{0;f_*}\\
&\quad\le h_{\tau_*}^{1/2}\|(\alpha\nabla\times(\boldsymbol{v}_{\mathcal{T}_*}-\boldsymbol{v}_{\mathcal{T}}))|_{\tau_*^1}\|_{0;f_*} + h_{\tau_*}^{1/2}\|(\alpha\nabla\times(\boldsymbol{v}_{\mathcal{T}_*}-\boldsymbol{v}_{\mathcal{T}}))|_{\tau_*^2}\|_{0;f_*}\\
&\quad\le h_{\tau_*}^{1/2}\|\alpha\|_{\infty,\tau_*^1\cup\tau_*^2}\Big(\|(\nabla\times(\boldsymbol{v}_{\mathcal{T}_*}-\boldsymbol{v}_{\mathcal{T}}))|_{\tau_*^1}\|_{0;f_*} + \|(\nabla\times(\boldsymbol{v}_{\mathcal{T}_*}-\boldsymbol{v}_{\mathcal{T}}))|_{\tau_*^2}\|_{0;f_*}\Big)\\
&\quad\lesssim \|\alpha\|_{\infty,\tau_*^1\cup\tau_*^2}\|\nabla\times(\boldsymbol{v}_{\mathcal{T}_*}-\boldsymbol{v}_{\mathcal{T}})\|_{0;\tau_*^1\cup\tau_*^2}.
\end{aligned}\tag{4.16}$$

Substituting (4.16) into (4.15), we obtain

$$h_{\tau_*}^{1/2}\|J_1(\boldsymbol{v}_{\mathcal{T}_*})\|_{0;f_*} \lesssim h_{\tau_*}^{1/2}\|J_1(\boldsymbol{v}_{\mathcal{T}})\|_{0;f_*} + \eta_{\mathcal{T}_*}(\boldsymbol{D},\tau_*)\|\nabla\times(\boldsymbol{v}_{\mathcal{T}_*}-\boldsymbol{v}_{\mathcal{T}})\|_{0;\tau_*^1\cup\tau_*^2}. \tag{4.17}$$

Using the definition of $J_1(\boldsymbol{v}_{\mathcal{T}_*})$ and the triangle inequality, we have

$$h_{\tau_*}^{1/2}\|J_2(\boldsymbol{v}_{\mathcal{T}_*})\|_{0;f_*} \le h_{\tau_*}^{1/2}\|J_2(\boldsymbol{v}_{\mathcal{T}})\|_{0;f_*} + h_{\tau_*}^{1/2}\|[\![\beta(\boldsymbol{v}_{\mathcal{T}_*}-\boldsymbol{v}_{\mathcal{T}})\cdot\boldsymbol{n}]\!]\|_{0;f_*}. \tag{4.18}$$

Similar to the proof of (4.16), we obtain

$$\begin{aligned}
&h_{\tau_*}^{1/2}\|[\![\beta(\boldsymbol{v}_{\mathcal{T}_*}-\boldsymbol{v}_{\mathcal{T}})\cdot\boldsymbol{n}]\!]\|_{0;f_*}\\
&\quad\le h_{\tau_*}^{1/2}\left(\|(\beta(\boldsymbol{v}_{\mathcal{T}_*}-\boldsymbol{v}_{\mathcal{T}}))|_{\tau_*^1}\|_{0;f_*} + \|(\beta(\boldsymbol{v}_{\mathcal{T}_*}-\boldsymbol{v}_{\mathcal{T}}))|_{\tau_*^2}\|_{0;f_*}\right)\\
&\quad\le h_{\tau_*}^{1/2}\|\beta\|_{\infty,\tau_*^1\cup\tau_*^2}\left(\|(\boldsymbol{v}_{\mathcal{T}_*}-\boldsymbol{v}_{\mathcal{T}})|_{\tau_*^1}\|_{0;f_*} + \|(\boldsymbol{v}_{\mathcal{T}_*}-\boldsymbol{v}_{\mathcal{T}})|_{\tau_*^2}\|_{0;f_*}\right)\\
&\quad\lesssim \|\beta\|_{\infty,\tau_*^1\cup\tau_*^2}\|\boldsymbol{v}_{\mathcal{T}_*}-\boldsymbol{v}_{\mathcal{T}}\|_{0;\tau_*^1\cup\tau_*^2}.
\end{aligned}\tag{4.19}$$

Substituting (4.19) into (4.18) implies

$$h_{\tau_*}^{1/2}\|J_2(\boldsymbol{v}_{\mathcal{T}_*})\|_{0;f_*} \lesssim h_{\tau_*}^{1/2}\|J_2(\boldsymbol{v}_{\mathcal{T}})\|_{0;f_*} + \eta_{\mathcal{T}_*}(\boldsymbol{D},\tau_*)\|\boldsymbol{v}_{\mathcal{T}_*}-\boldsymbol{v}_{\mathcal{T}}\|_{0;\tau_*^1\cup\tau_*^2}. \tag{4.20}$$

Squaring both sides of (4.13), (4.14), (4.17) and (4.20), applying Young's inequality $2ab \le \epsilon a^2 + \epsilon^{-1}b^2$, summing all elements $\tau_*$ and interior faces $f_*$ and observing the monotonicity of local mesh sizes and the shape regularity of the mesh $\mathcal{T}$ and (4.9), we get the desired inequality (4.10). ∎

We then prove the contraction of the error estimator if the solution does not change.

**Lemma 4.5** *Given a $\theta \in (0,1)$, let $\mathcal{T}_*$ be a conforming and shape regular triangulation which is refined from a conforming and shape regular triangulation $\mathcal{T}$ using the Dörfler marking strategy (3.7). Let $\boldsymbol{u}_{\mathcal{T}} \in \mathbb{V}(\mathcal{T})$ be the discrete solution of (1.3). Then there exists a constant $\gamma \in (0,1)$, such tat*

$$\eta^2(\boldsymbol{u}_{\mathcal{T}},\mathcal{T}_*) \le \gamma\eta^2(\boldsymbol{u}_{\mathcal{T}},\mathcal{T}). \tag{4.21}$$

**Proof.** We shall divide the proof into two steps. In the first step, we prove the element-wise contraction if one element is divided into at least two parts, and in the second step, we shall use the Dörfler marking to prove the global version.

*Step 1.* Suppose $\tau \in \mathcal{T}$ is bisected into $\tau_*^1 \in \mathcal{T}_*$ and $\tau_*^2 \in \mathcal{T}_*$. We shall prove that there exists a number $\bar{\gamma} \in (0,1)$, such that

$$\eta^2_{\mathcal{T}_*}(\boldsymbol{u}_{\mathcal{T}}, \tau_*^1) + \eta^2_{\mathcal{T}_*}(\boldsymbol{u}_{\mathcal{T}}, \tau_*^2) \le \bar{\gamma}\eta^2_{\mathcal{T}}(\boldsymbol{u}_{\mathcal{T}}, \tau). \tag{4.22}$$

In fact, by the definition of the mesh size $h^3_{\tau_*^1} = |\tau_*^1| = |\tau_*^2| = h^3_{\tau_*^2} = \frac{1}{2}h^3_\tau$, the element wise residual is reduced:

$$h^2_{\tau_*^1}\|R_j(\boldsymbol{u}_{\mathcal{T}})\|^2_{0,\tau_*^1} + h^2_{\tau_*^2}\|R_j(\boldsymbol{u}_{\mathcal{T}})\|^2_{0,\tau_*^2} = 2^{-2/3}h^2_\tau\|R_j(\boldsymbol{u}_{\mathcal{T}})\|^2_{0,\tau}, j = 1,2. \tag{4.23}$$

On the jump residual associated with faces, we note that after $\tau$ is bisected, in $\tau_*^1$ and $\tau_*^2$, there are three types of faces.

1. For the new face created by the bisection, which is inside the element $\tau$, the function $\boldsymbol{u}_{\mathcal{T}}$ is a polynomial and coefficients are continuous. Therefore $[\![(\alpha\nabla \times \boldsymbol{u}_{\mathcal{T}}) \times \boldsymbol{n}]\!]$ and $[\![(\boldsymbol{g} - \beta\boldsymbol{u}_{\mathcal{T}}) \cdot \boldsymbol{n}]\!]$ are zero.

2. For the faces divided from $\tau$, the jump values are invariant. But the mesh size is decreased by $2^{-1/3}$ as in the case of element-wise residual.

3. For the faces unchanged or inherited from $\tau$, also the jump values are invariant but the mesh size is decreased by $2^{-1/3}$. The crucial observation is that we use the mesh size $h_\tau$ in the jump residual.

*Step 2.* Let $\mathcal{M} \subset \mathcal{T}$ be the marked set by using the marking strategy (3.7). We may need to refine more elements in order to recover the conformity of the triangulation and thus denote the set of refined elements as $\mathcal{R}_{\mathcal{T}\to\mathcal{T}_*}$. Since $\mathcal{M} \subseteq \mathcal{R}_{\mathcal{T}\to\mathcal{T}_*}$, we have $\eta^2(\boldsymbol{u}_{\mathcal{T}}, \mathcal{R}_{\mathcal{T}\to\mathcal{T}_*}) \ge \theta\eta^2(\boldsymbol{u}_{\mathcal{T}}, \mathcal{T})$. We use $\overline{\mathcal{R}_{\mathcal{T}\to\mathcal{T}_*}} \subset \mathcal{T}_*$ to denote the set of new elements refined from $\mathcal{R}_{\mathcal{T}\to\mathcal{T}_*}$. Obviously, $\mathcal{T}\backslash\mathcal{R}_{\mathcal{T}\to\mathcal{T}_*} = \mathcal{T}_*\backslash\overline{\mathcal{R}_{\mathcal{T}\to\mathcal{T}_*}}$ are unchanged elements.

Using (4.22) and the marking strategy (3.7), we have

$$\begin{aligned}
\eta^2(\boldsymbol{u}_{\mathcal{T}}, \mathcal{T}_*) &= \eta^2(\boldsymbol{u}_{\mathcal{T}}, \mathcal{T}_*\backslash\overline{\mathcal{R}_{\mathcal{T}\to\mathcal{T}_*}}) + \eta^2(\boldsymbol{u}_{\mathcal{T}}, \overline{\mathcal{R}_{\mathcal{T}\to\mathcal{T}_*}}) \\
&\le \eta^2(\boldsymbol{u}_{\mathcal{T}}, \mathcal{T}\backslash\mathcal{R}_{\mathcal{T}\to\mathcal{T}_*}) + \bar{\gamma}\eta^2(\boldsymbol{u}_{\mathcal{T}}, \mathcal{R}_{\mathcal{T}\to\mathcal{T}_*}) \\
&= \eta^2(\boldsymbol{u}_{\mathcal{T}}, \mathcal{T}) + (\bar{\gamma} - 1)\eta^2(\boldsymbol{u}_{\mathcal{T}}, \mathcal{R}_{\mathcal{T}\to\mathcal{T}_*}) \\
&\le \eta^2(\boldsymbol{u}_{\mathcal{T}}, \mathcal{T}) + \theta(\bar{\gamma} - 1)\eta^2(\boldsymbol{u}_{\mathcal{T}}, \mathcal{T}) \\
&= \gamma\eta^2(\boldsymbol{u}_{\mathcal{T}}, \mathcal{T}),
\end{aligned}$$

with $\gamma = 1 + \theta(\bar{\gamma} - 1) \in (0,1)$, this completes the proof of (4.21). ∎

In the end of this subsection, we will prove the contraction of error estimator using Lemmas 4.4 and 4.5.

**Lemma 4.6** *There exists $\xi \in (0,1)$ depending only on the shape regularity of $\mathcal{T}_k$ and the parameter $\theta$ used in the marking strategy, such that*

$$\eta^2(\boldsymbol{u}_{k+1}, \mathcal{T}_{k+1}) \le \xi\eta^2(\boldsymbol{u}_k, \mathcal{T}_k) + C_\xi\eta^2(\boldsymbol{D}, \mathcal{T}_0)\|\boldsymbol{u}_{k+1} - \boldsymbol{u}_k\|^2_A, \tag{4.24}$$

*where the constant $C_\xi$ depends only on $\xi$, $c_a^{-1}$ and the shape regularity of $\mathcal{T}_0$.*

**Proof.** Let $\mathcal{T} = \mathcal{T}_k$ and $\mathcal{T}_* = \mathcal{T}_{k+1}$ in Lemma 4.4 and Lemma 4.5, then the desired result (4.24) follows by choosing $\epsilon$ small enough such that $\xi = (1+\epsilon)\gamma < 1$. ∎

## 4.4 Convergence result

Now we are in position to present and prove the contraction of the summation of the energy error and the scaled error estimate. Similar to the elliptic equations cases, each term of the summation may not strictly decay. The corresponding discussion for elliptic equations can be found in [18].

**Theorem 4.7** *For a given $\theta \in (0,1)$, let $\{\mathcal{T}_k, \mathbb{V}(\mathcal{T}_k), \boldsymbol{u}_k, \eta(\boldsymbol{u}_k, \mathcal{T}_k)\}_{k\geq 0}$ be the sequence of meshes, finite element spaces, discrete solutions and error estimates produced by the AEFEM. Then there exist constants $\rho > 0$, and $\delta \in (0,1)$, depending only on $\theta$, the shape regularity of $\mathcal{T}_0$, the coefficients $\alpha$ and $\beta$, such that*

$$\|\boldsymbol{u} - \boldsymbol{u}_{k+1}\|_A^2 + \rho\, \eta^2(\boldsymbol{u}_{k+1}, \mathcal{T}_{k+1}) \leq \delta \left( \|\boldsymbol{u} - \boldsymbol{u}_k\|_A^2 + \rho\, \eta^2(\boldsymbol{u}_k, \mathcal{T}_k) \right).$$

**Proof.** We fix a $\xi \in (0,1)$ in Lemma 4.6 and let $\rho = (C_\xi \eta^2(\boldsymbol{D}, \mathcal{T}_0))^{-1}$. Suppose $\delta \in (0,1)$ which will be determined later. By adding $\rho\, \eta^2(\boldsymbol{u}_{k+1}, \mathcal{T}_{k+1})$ to both sides of (4.1), then splitting $\delta\|\boldsymbol{u} - \boldsymbol{u}_k\|_A^2$ and applying Lemma 4.6 to cancel $\|\boldsymbol{u}_{k+1} - \boldsymbol{u}_k\|_A^2$, we obtain

$$\begin{aligned}
&\|\boldsymbol{u} - \boldsymbol{u}_{k+1}\|_A^2 + \rho\, \eta^2(\boldsymbol{u}_{k+1}, \mathcal{T}_{k+1}) \\
&\quad = \|\boldsymbol{u} - \boldsymbol{u}_k\|_A^2 - \|\boldsymbol{u}_{k+1} - \boldsymbol{u}_k\|_A^2 + \rho\, \eta^2(\boldsymbol{u}_{k+1}, \mathcal{T}_{k+1}) \\
&\quad \leq \delta\|\boldsymbol{u} - \boldsymbol{u}_k\|_A^2 + (1-\delta)\|\boldsymbol{u} - \boldsymbol{u}_k\|_A^2 + \rho\xi\eta^2(\boldsymbol{u}_k, \mathcal{T}_k) \\
&\quad \leq \delta \left( \|\boldsymbol{u} - \boldsymbol{u}_k\|_A^2 + \frac{(1-\delta)C_1 + \rho\xi}{\delta} \eta^2(\boldsymbol{u}_k, \mathcal{T}_k) \right),
\end{aligned} \tag{4.25}$$

In the last step, we apply Lemma 4.3 to $\|\boldsymbol{u} - \boldsymbol{u}_k\|_A^2$.

This leads us to choose $\delta$, such that

$$\rho = \frac{(1-\delta)C_1 + \rho\xi}{\delta}. \tag{4.26}$$

Namely

$$\delta = \frac{C_1 + \rho\xi}{C_1 + \rho} < 1, \tag{4.27}$$

which completes the proof. ∎

By recursion, we get the decay of the error and the estimator.

**Corollary 4.8** *Under the hypotheses of Theorem 4.7, we have*

$$\|\boldsymbol{u} - \boldsymbol{u}_k\|_A^2 + \rho\, \eta^2(\boldsymbol{u}_k, \mathcal{T}_k) \leq \hat{C}_0 \delta^k,$$

*where the constants $\rho$ and $\delta$ are given in Theorem 4.7, and $\hat{C}_0 := \|\boldsymbol{u} - \boldsymbol{u}_0\|_A^2 + \rho\, \eta^2(\boldsymbol{u}_0, \mathcal{T}_0)$. Thus the algorithm AEFEM will terminate in finite steps.*

# 5 Numerical Experiments

In this section, we present some numerical examples to show the efficiency and robustness of AEFEM.

In example 1, we choose an "L-shaped" domain $\Omega = (-1,1)^3/([0,1)\times[0,1)\times(-1,1))$ and get an initial mesh $\mathcal{T}_0$ by partitioning the $x-, y-$ and $z-$axes into equally distributed 4 subintervals, and then dividing one cube into six tetrahedron; see the left of Figure 1. The Dirichlet boundary condition and the source $\boldsymbol{g}$ are chosen such that the exact solution is $\boldsymbol{u} = \mathbf{grad}(r^{\frac{2}{3}}\sin(\frac{2}{3}\theta))$ (in cylindrical coordinates) and the coefficients $\alpha = \beta = 1$. The finite element space $\boldsymbol{V}(\mathcal{T}_h) = \boldsymbol{V}^{1,1}(\mathcal{T}_h)$. The three-dimensional local refinement is adapted from $i$FEM [9].

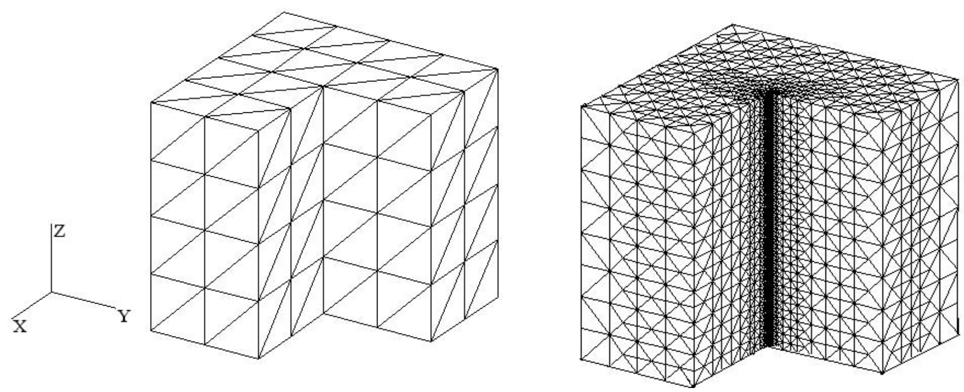


Figure 1: The initial mesh $\mathcal{T}_0$ (left). An adaptively refined mesh after 17 adaptive iterations with marking parameter $\theta = 0.5$ (right).

The right of Figure 1 shows an adaptively refined mesh with marking parameter $\theta = 0.5$ after $k = 17$ iteration steps. The mesh is locally refined in a small vicinity of the edge singularity. Figure 2 shows the curves of $\ln \#\mathcal{T}_k - \ln \|\boldsymbol{u} - \boldsymbol{u}_k\|_A$ for different marking parameters $\theta$, where $\#\mathcal{T}_k$ is the number of elements and $\boldsymbol{u}_k$ is the corresponding finite element solution associated to the mesh $\mathcal{T}_k$. These curves indicate the convergence and the quasi-optimality of adaptive mesh refinements of the energy error $\|\boldsymbol{u} - \boldsymbol{u}_k\|_A$, i.e.

$$\|\boldsymbol{u} - \boldsymbol{u}_k\|_A \le C(\#\mathcal{T}_k)^{-1/3}.$$

In example 2, we consider the adaptive refinement process in the case of discontinuous coefficients. We choose the cube $\Omega = (-1,1)^3$ as the computational domain, and set the homogeneous Dirichlet boundary condition $\boldsymbol{n}_{\partial\Omega} \times \boldsymbol{u} = \boldsymbol{0}$ on $\partial\Omega$, the source $\boldsymbol{g} = 1$, and the coefficients $\alpha$ and $\beta$

$$\begin{cases} \alpha = 1.0,\ \beta = 1.0 & \text{on } \Omega_1, \\ \alpha = 1.0,\ \beta = 100 & \text{on } \Omega \setminus \Omega_1, \end{cases}$$

where $\Omega_1 = (-0.5, 0.5)^3$. The jump of the coefficient $\beta$ is on the boundary of the floating subdomains $\Omega_1$, which was reported to be problematic for geometric multigrid in [14].

We test the performance of AEFEM for different finite element spaces. Figure 3 shows the curves of $\ln \#\mathcal{T}_k - \ln \|\boldsymbol{u} - \boldsymbol{u}_k\|_A$ for different types Nédélec linear element spaces using the same marking parameters $\theta = 0.5$, respectively. Here, we use $\|\boldsymbol{u}_{17} - \boldsymbol{u}_k\|_A$ $(0 \le k \le 13)$ and $\|\boldsymbol{u}_{16} - \boldsymbol{u}_k\|_A$ $(0 \le k \le 12)$ to approxiamte $\|\boldsymbol{u} - \boldsymbol{u}_k\|_A$, since the exact solution $\boldsymbol{u}$ is unknown. Since the finest mesh is small enough, this choice is reasonable. Figure 3 also indicates the convergence and quasi-optimality of AEFEM.

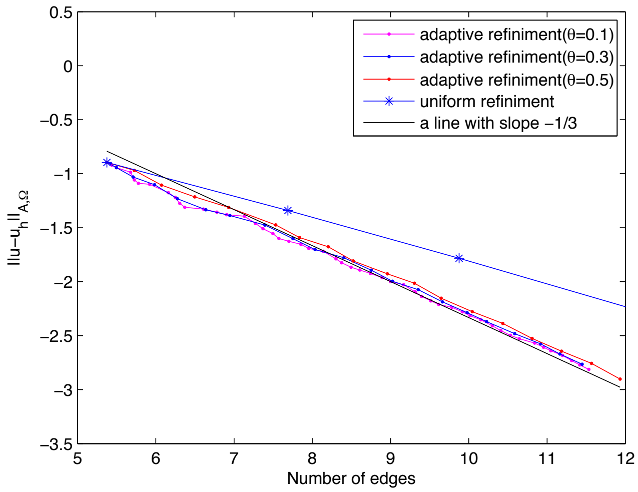


Figure 2: Quasi optimality of the adaptive mesh refinements of the error $\|\boldsymbol{u} - \boldsymbol{u}_k\|_A$ with different marking parameters $\theta$ and $\boldsymbol{V}(\mathcal{T}_h) = \boldsymbol{V}^{1,1}(\mathcal{T}_h)$..

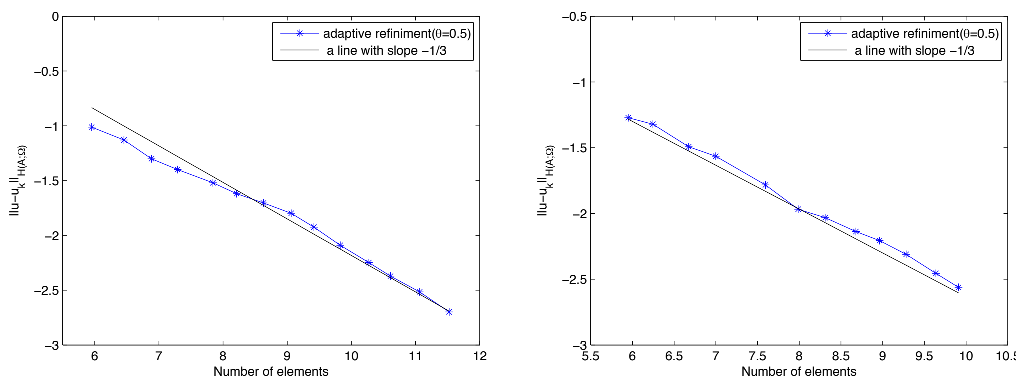


Figure 3: $\boldsymbol{V}(\mathcal{T}_h) = \boldsymbol{V}^{1,1}(\mathcal{T}_h)$ (left). $\boldsymbol{V}(\mathcal{T}_h) = \boldsymbol{V}^{1,2}(\mathcal{T}_h)$ (right).

Figures 4 and 5 show the $(x; y)$-cross sections at the different values of $z$ of the adaptively refined grid after 12 refinement steps for $\theta = 0.5$. The meshes are locally refined in the region of singularity, which is symmetric with respect to the origin, but the region of polluted elements for first type Nédélec linear element spaces is larger than that for second type Nédélec linear element spaces.

We then test the performance of AEFEM for first type Nédélec quadratic element spaces with different marking parameters $\theta$. The left Figure 6 shows the convergence of the error in the energy norm and its quasi-optimality $\|\boldsymbol{u} - \boldsymbol{u}_k\|_A \leq C(\#\mathcal{T}_k)^{-2/3}$ after several steps. From these curves, it seems that the convergence and the convergent rate is robust for $\theta$ changing from 0.1 to 0.5. The inflection point of curves could depend on the regularity of the real solution. We plot several $(x; y)$-cross sections at the different values of $z$ of the

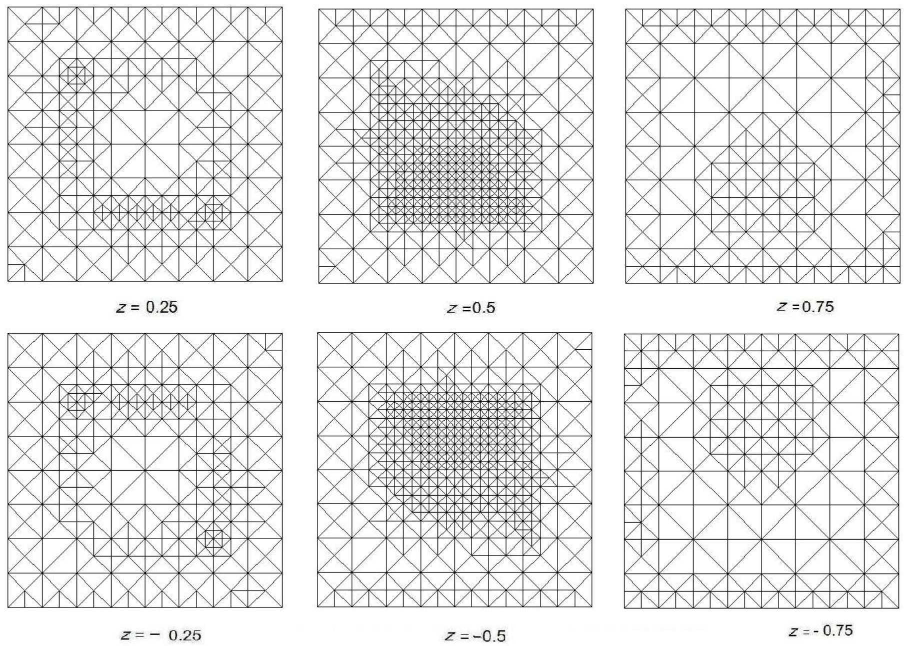


Figure 4: Cross section ($(x;y)$-plane) at the different values of $z$ of the adaptively refined grid for $\boldsymbol{V}(\mathcal{T}_h) = \boldsymbol{V}^{1,1}(\mathcal{T}_h)$.

adaptively refined grid after 11 refinement steps for $\theta = 0.5$ in Figure 7. It shows that the region of polluted elements for this case is smaller than that for linear element spaces.

To show the effect from the discontinuity of the coefficients, we present the error curves for smooth coefficients $\alpha = \beta = 1$ and $\theta = 0.5$ in the right of Figure 6 using the same quadratic edge element space $\boldsymbol{V}^{2,1}(\mathcal{T}_h)$. In this case, since the coefficients and the source are smooth and the domain is convex, the full regularity result holds. Therefore the error decay in an optimal rate from the every beginning.

For any $\theta \in (0,1)$, the algorithm AEFEM will converge from our theoretical results. But according to the theoretical results of optimal rate of convergence [8, 24], to achieve optimal convergence, the marking parameter $\theta$ should be less than $\theta^*$, a value depending on the quality of the a posteriori error estimator and the degree of polynomials. In our numerical experiments, we restrict theta to be less than or equal to 0.5. The theoretical investigation of the optimality of AEFEM will be reported in a future work.

**Acknowledgments.** The authors would like to thank Chunmei Liu from Xiangtan University, for her help with the numerical experiments. The authors are also grateful to the referees for their constructive comments which improve the presentation of the paper. The first and second author were supported in part by National Natural Science Foundation of China (Grant No. 10771178 and 10676031), National Key Basic Research Program of China (973 Program) (Grant No. 2005CB321702), the Key Project of Chinese Ministry of Education and Scientific Research Fund of Hunan Provincial Education Department (Grant No. 208093 and 07A068). The third author was supported in part by NSF Grant DMS-0811272 and NIH Grants P50GM76516 and R01GM75309. The last author was partially supported

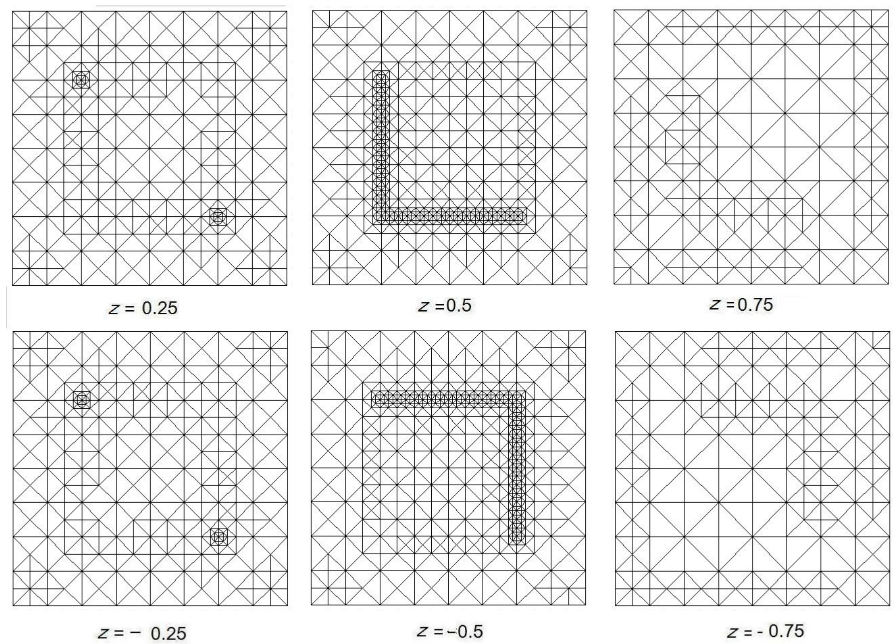


Figure 5: Cross section ($(x;y)$-plane) at the different values of $z$ of the adaptively refined grid for $\boldsymbol{V}(\mathcal{T}_h) = \boldsymbol{V}^{1,2}(\mathcal{T}_h)$.

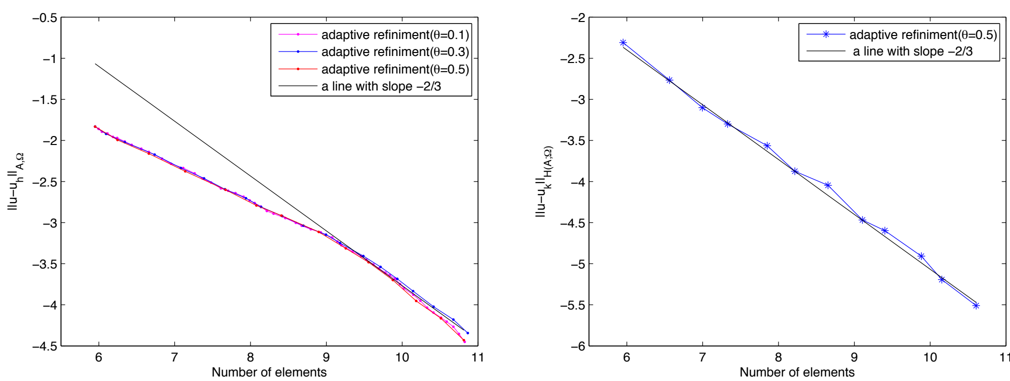


Figure 6: Numerical simulation using $\boldsymbol{V}(\mathcal{T}_h) = \boldsymbol{V}^{2,1}(\mathcal{T}_h)$. Quasi optimality of the adaptive mesh refinements with discontinuous coefficients and different marking parameters $\theta$(left). Quasi optimality of the adaptive mesh refinements with with continuous coefficients and $\theta = 0.5$(right).

by Alexander von Humboldt Research Award for Senior US Scientists, NSF DMS-0609727, NSFC-10528102.

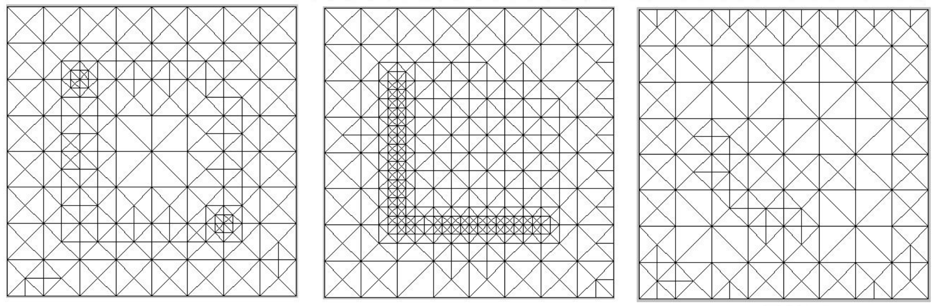


Figure 7: Cross section ($(x;y)$-plane) at the different values of $z$ of the adaptively refined grid after 15 refinement steps for $\theta = 0.5$ and $\boldsymbol{V}(\mathcal{T}_h) = \boldsymbol{V}^{2,1}(\mathcal{T}_h)$.

# References


[1] L.S. Andersen and J.L. Volakis. Adaptive multiresolution antenna modeling using hierarchical mixed-order tangential vector finite elements. *IEEE Trans. Antennas Propag.*, 49(2):211–222, 2001.

[2] D.N. Arnold, R.S. Falk, and R. Winther. Multigrid in $H(div)$ and $H(curl)$. *Numer. Math.*, 85(2):197–217, 2000.

[3] R. Beck, P. Deuflhard, R. Hiptmair, R.H.W Hoppe, and B. Wohlmuth. Adaptive multilevel methods for edge element discretizations of Maxwell's equations. *Surveys Math. Industry*, 8:271–312, 1999.

[4] R. Beck, R. Hiptmair, R.H.W. Hoppe, and B. Wohlmuth. Residual based a posteriori error estimators for eddy current computation. *M2AN Math. Model. Numer. Anal.*, 34(1):159–182, 2000.

[5] R. Beck, R Hiptmair, and B. Wohlmuth. Hierarchical error estimator for eddy current computation. In *In ENUMATH99: Proceedings of the 3rd European Conference on Numerical Mathematics and Advanced Applictions (ed. P. Neitaanmaki and T. Tiihonen), 110-120. World Scientific, Singapore,*, 2000.

[6] A. Bossavit. *Computational Electromagnetism. Variational Formulation, Complementarity, Edge Elments.* vol. 2 of Electromagnetism Series. Academic Press, San Diego, CA, 1998.

[7] C. Carstensen and R.H.W Hoppe. Convergence analysis of an adaptive edge finite element method for the 2D eddy current equations. *J. Numer. Math.*, 13(1):19–32, 2005.

[8] J.M. Cascon, C. Kreuzer, R.H. Nochetto, and K.G. Siebert. Quasi-optimal convergence rate for an adaptive finite element method. *SIAM J. Numer. Anal.*, 46:2524–2550, 2008.

[9] L. Chen. $i$FEM: an innovative finite element methods package in MATLAB. Submitted, 2008.

[10] L. Chen, R.H. Nochetto, and J. Xu. Multilevel methods on graded bisection grids II: $H(curl)$ and $H(div)$ systems. Preprint, 2008.

[11] P. G. Ciarlet. *The Finite Element Method for Elliptic Problems*, vol. 4 of Studies in Mathematics and its Applications, North-Holland Publishing Co., Amsterdam-New York-Oxford, 1978.

[12] W. Dörfler. A convergent adaptive algorithm for poisson's equation. *SIAM J. Numer. Anal.*, 33(3):1106–1124, 1996.

[13] N.A. Golias and T.D. Papagiannakis, A.G. andTsiboukis. Efficient mode analysis with edge elements and 3-D adaptive refinement. *IEEE Trans. Microwave Theory Tech.*, MTT-42:99–107, 1994.

[14] R. Hiptmair. Multigrid method for Maxwell's equations. *SIAM J. Numer. Anal.*, 36(1):204–225, 1999.

[15] R. Hiptmair and W. Zheng. Local multigrid in $H(curl)$. *J. Comput. Math.*, 27(5):573–603, 2009.

[16] R.H.W. Hoppe and J. Schöberl. Convergence of adaptive edge element methods for the 3D eddy currents equations. *J. Comput. Math.*, 27(5):657–676, 2009.

[17] S. McFee and D. Giannacopoulos. Optimal discretization based refinement criteria for finite element adaption. *IEEE Trans. Magn.*, 32(3):1357–1360, 1996.

[18] P. Morin, R.H. Nochetto, and K.G. Siebert. Convergence of adaptive finite element methods. *SIAM Rev.*, 44(4):631–658, 2002.

[19] J.C. Nédélec. Mixed finite elements in $R^3$. *Numer. Math.*, 35:315–341, 1980.

[20] J.C. Nédélec. A new family of mixed finite elements in $R^3$. *Numer. Math.*, 50(1):57–81, 1986.

[21] J. Schöberl. Commuting quasi-interpolation operators for mixed finite elements. In *2nd European Conference on Computational Mechanics*, pages 854–855, 2001.

[22] J. Schöberl. A posteriori error estimates for Maxwell equations. *Math. Comp.*, 77:633–649, 2008.

[23] O. Sterz, A. Hauser, and G. Wittum. Adaptive local multigrid methods for the solution of Time Harmonic eddy current problems. *IEEE Trans. Magn.*, 42:309–318, 2006. Interdisciplineary Center for Scientific Computing of the University of Heidelberg 2005.

[24] R. Stevenson. Optimality of a standard adaptive finite element method. *Found. Comput. Math.*, 7(2):245–269, 2007.

[25] D.K. Sun, Z. Cendes, and J. F. Lee. Adaptive mesh refinement, $h$-version, for solving multi-port microwave devices in three dimensions. *IEEE Trans. Magn.*, 36:1596–1599, 2000.

[26] J.P. Webb and B. Forghani. Adaptive improvement of magnetic fields using hierarchal tetrahedral finite elements. *IEEE Trans. Magn.*, 30(5):3511–3514, 1994.

[27] J. Xu. Iterative methods by space decomposition and subspace correction. *SIAM Rev.*, 34(4):581–613, 1992.